



Journal of Mining and Environment (JME)

journal homepage:
www.jme.shahroodut.ac.ir



Accuracy of Discrete Element Method Simulations: Rolling and Sliding Frictions Effects-Case study: Iron Ore Pellets

Elham Nematollahi¹, Ali Reza Ghasemi¹, Erfan Razi² and Samad Banisi^{1*}

1. Mining Engineering Department, Shahid Bahonar University of Kerman, Kerman, Iran

2. Kashigar Mineral Processing Research Centre, Shahid Bahonar University of Kerman, Kerman, Iran

Article Info

Received 29 October 2020

Received in Revised form 16
November 2020

Accepted 22 November 2020

Published online 22 November
2020

DOI:10.22044/jme.2020.10208.1958

Keywords

DEM

Contact parameters

Repose angle

Calibration

Iron ore pellets

Abstract

The discrete element method (DEM) has been used as a popular simulation method in order to verify the designs by visualizing how materials flow through complex equipment geometries. Although DEM simulation is a powerful design tool, finding a DEM model that includes all real material properties is not computationally feasible. In order to obtain more realistic results, particle energy loss due to rolling friction has been highlighted by many researchers using various models to implement a reverse torque. On account of the complexity of the problem, there is no unique model for all applications (i.e. dynamic and pseudo-static regimes). In this research work, an in-house developed DEM software (KMPCDEM©) was used to assess the robustness of three models by comparing the repose angle obtained through the draw down test. The elastic-plastic spring dashpot model was then modified based on considering the individual parameters instead of the relative parameters of two contact entities. The results showed that the modified model could produce a higher repose angle. The modified model was used for the calibration of DEM input parameters in the simulation of repose angle of iron ore pellets in a laboratory setup of the draw down test. Comparison of the calibrated DEM simulation (using 0.0007 and 0.75 for the rolling and sliding friction coefficients, respectively) with the laboratory results showed a good agreement between the predicted and measured angle of repose. The non-calibrated DEM simulations are susceptible to error, and therefore, it is strongly recommended to use the laboratory experiments to characterize the materials before using the DEM simulation as a design tool of industrial equipment.

1. Introduction

1.1. Discrete element method (DEM)

It has been about 40 years since the original development [1] of the discrete method (DEM) and now it is used with numerous granular assembly applications [2-4]. DEM simulation provides a basic understanding of the processes under the controlled conditions [5]. This understanding of the process can also help to modify the strategy of processes, prevent the test prototypes, identify the deficiencies in equipment design, and likely, redesign of some equipment [6-8]. Hence, almost no design could be accepted for the construction stage without verification by numerical simulation

methods (i.e., DEM) or pilot testing. Although DEM simulation is a powerful design tool, finding a DEM model that includes real material properties (e.g., shape, cohesion and friction coefficients) is not computationally feasible [6]. A real bulk material, for example, a typical conveyor belt [9], is composed of millions of particles with very varied physical and dynamic features, different shapes and size distributions. Despite all the improvements in DEM such as evolution of contact models and attempts to utilize the more realistic particles [10], DEM requires a high degree of simplifications. Therefore, the accuracy of the DEM simulation results and their degree of

✉ Corresponding author: Banisi@uk.ac.ir (S. Banisi).

reliability for application in designs depends on the ability of finding a representative model for the bulk materials. Since the bulk behavior of a particle system is affected by the collective interactions of individual particles, it is very useful to study the material behavior on the particle scale which is the primary concern of this paper.

1.1.1. Modelling particle behavior in DEM

In DEM, movements of particles (that are considered as spheres, for simplicity) falls into two groups: free falling and colliding states [7, 11]. Figure 1-a shows an *i*th contact between the particles A and B in the contact point of C. A contact force (F_i) is working, which is decomposed to normal (N_i) and tangential (T_i) components [12]. The in-depth presentations of the mathematical formulation and computer implementation can be found elsewhere [11].

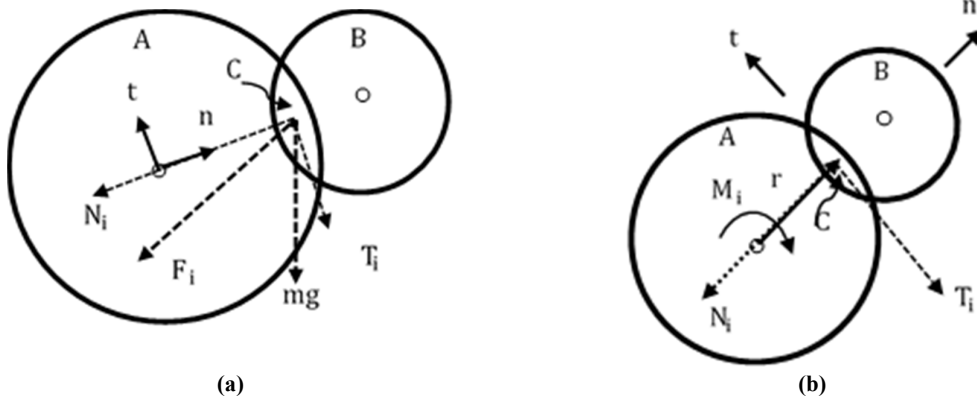


Figure 1. A 2D illustration of forces acting on particle A in contact with particle B, a) translational and b) rotational motions (Zhou et al., 1999 [13]).

Generally, the contact deformation and rolling are two phenomena that may occur in the contact between two particles [14]. The former is usually separated into relative translations (including both normal and tangential) and relative rotations. The relative tangential deformation is called sliding. The governing equation for the translational motion of particle A (shown in Figure1-a) can be written as [12]:

$$m \frac{dV}{dt} = mg + \sum_{i=1}^n (N_i + T_i) \tag{1}$$

where *m* and *V* are the mass and velocity of particle A, respectively, and *t* is time. Besides the contact force, another force acting on particle A is the gravitational force, *mg*. Since the forces act at the contact point between particles A and B rather than the particle center, a torque (M_i , shown in Figure1-b) will generate, causing particle A to rotate [13]. Thus, the governing equation for the rotational motion of particle A is:

$$\sum_{i=1}^k r \times T_i = I \frac{d\omega}{dt} \tag{2}$$

where ω is the angular velocity, and *I* is the moment of inertia of particle A. In addition to the translational and rotational motions, two particles may roll across each other. The translational and rotational motions are clear, but this is not the case for the rolling. The composition of the translation of particle centroids and the rotations of the particles about their centroids is called rolling motion. It has generally been accepted that particle rolling is a major microscopic deformation mechanism during the flow of cohesionless granular materials [12, 13].

In DEM simulation, where the particles are considered spherical, the particles collide in a single contact point which makes them rolls freely [12, 15]. The free rolling feature makes particles move continuously which makes the formation of a stable heap impossible, and finally, a flatten shape is obtained [2, 5, 13]. On the other hand, a problem of steady movement by rolling is that the flow behavior developed in this simulation is completely different from that observed in the natural processes. The difference seems to be originated from a lack of rolling friction (or rolling resistance in some literature) at contacts. Hysteresis at the contact point and the effect of shape are two main sources that contribute to

energy loss due to rolling in real physical systems [9, 16]. The former is of importance for granular materials, however, in practice, the effect of shape is the predominant effect [9, 17, 18].

Figure 2 illustrates the effect of shape on the energy loss of particles. When two circular particles are in contact, the contact point is always in the same direction of the line connecting the

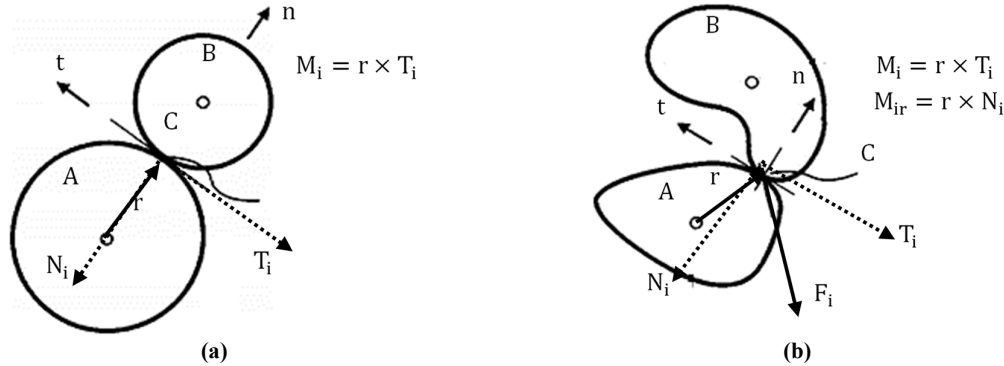


Figure 2. Calculation of torque for, a) two circular particles and b) arbitrary 2D particles (Bagi and Kuhn, 2004 [14]).

As it was stated, the shape plays an important role in the behavior of granular materials, but it is a complex factor to model in DEM [9]. As a result, using the rolling friction as a simple way to introduce shape-like behavior has been highlighted by many researchers [2, 9, 16, 17, 19, 20-23]. Consequently, they have attempted to express a reverse torque for rolling friction using different models. In order to implement the idea, the conservation law of angular momentum for the particle (i.e., Equation 2) is rewritten as:

$$\sum_{i=1}^k (r \times T_i + M_{ir}) = I \frac{d\omega}{dt} \quad (3)$$

1.1.2. Application of rolling friction in DEM

Six model types are commonly used to form a resistive torque and consequently the rolling friction in DEM.

Group A models: In these cases, only the direction of relative angular velocity of the particles forming the contact is important [13, 24, 25]. The rolling resistance torque, M_r , is defined as;

$$M_r = -\frac{\omega_{rel}}{|\omega_{rel}|} \mu_r R_r F_n \quad (4)$$

where, μ_r , F_n , ω_{rel} and R_r are the rolling friction coefficient, contact normal force, relative angular velocity of the particles forming the contact and effective radius, respectively.

centers of two particles (i.e., normal direction). In this case, the normal force could not produce a torque that could resist to rolling. For the case of two arbitrary particles (with real shape), both the tangential and normal forces could create torque. The former causes the rotation of particle and the latter acts to oppose rolling motion [14].

Group B models: Despite the above models, both magnitude and direction of relative angular (or translational) velocity at the contact due to rolling are important [5]. The resistive torque in type B models is of the form;

$$M_r = -\mu_r R_r F_n (\omega_i r_i - \omega_j r_j) \quad (5)$$

Group C models: Is a class of elastic-plastic spring dashpot models that composites the elastic and viscous parts [14, 16, 26, 27]. The general form of group C models is defined by Equation (6).

$$M_r = M_r^k + M_r^d \quad (6)$$

The elastic part of the group C models rolling resistance (ΔM_r^k) is defined in an incremental way by the following;

$$\Delta M_r^k = -k_r \omega_{rel} \Delta t \quad (7)$$

where k_r is a parameter known as the rolling stiffness that characterizes the compliance (defined as $2J_n R_r F_n$ with J_n being a dimensionless coefficient that varies theoretically from 0.25 to 0.5 and found to be close to 0.5 for hard particles on a flat surface [16].) and Δt is the time step in DEM calculations. The cumulative form of Equation (7) is:

$$\begin{cases} M_{r,t+\Delta t}^k = M_{r,t}^k + \Delta M_r^k \\ |M_{r,t+\Delta t}^k| \leq M_r^m \end{cases} \quad (8)$$

Where

$$M_r^m = \mu_r R_r F_n \tag{9}$$

is the limiting spring torque that is achieved at a full mobilization rolling angle.

The viscous component (M_r^d) is of the form:

$$M_{r, t+\Delta t}^d = \begin{cases} -C_r \omega_{rel}, & \& |M_{r, t+\Delta t}^d| < M_r^m \\ 0, & otherwise \end{cases} \tag{10}$$

where the damping rate (C_r) is defined as $C_r = 2\eta_r \sqrt{I_r k_r}$, with I_r being the equivalent moment of inertia and η_r being the rolling viscous damping ratio.

Group D models: These models tend to apply a resistive torque that is related to the angular velocity of each individual particle (i.e., ω_i or ω_j) rather than the relative behavior of a pair of contacting particles [15, 19]. Equation (11) describes one example of this type of rolling friction models.

$$M_i = -\mu_r F_{ij}^{c,n} \frac{\omega_i}{|\omega_i|}; M_j = -\mu_r F_{ij}^{c,n} \frac{\omega_j}{|\omega_j|} \tag{11}$$

Group E models: These models are related to the rolling velocity (V_r ; defined in Equation (12)). The form of these models is given by Equation (13).

$$V_r = -R_r n \times (\omega_i - \omega_j) \tag{12}$$

with the unit vector n pointing from the center of particle j to the center of particle i .

$$M_r = k_r V_r \Delta t; k_r V_r \Delta t \leq \mu_r F_n \tag{13}$$

Group F models: The force base models are defined as:

$$M_r = R_r n \times R_k \tag{14}$$

The rolling force (R_k) can be computed as two following equations:

$$R_k = \text{sgn}(-V_{rel}) \times \min(\gamma_s m_{ij} |V_{rel}|, \mu_s |N_k|); V_{rel} = r \times (\omega_i + \omega_j) \tag{15-a}$$

$$R_k = \frac{R_{o,k}}{|R_{o,k}|} \times \min(|R_{o,k}|, \mu_r |N_k|) \tag{15-b}$$

$$R_{o,k} = -k_r \Delta U_r - C_r V_r$$

To the best of our knowledge, all the major types of rolling friction models used in DEM simulations could be classified in one of the six outlined model groups. It has also been reported the successful application of almost all models to reproduce the real results by various researchers [9, 13, 20, 24, 27-30]. In general, the difference between the rolling friction models arises from the nature of the specific problem studied. For instance, some of these models have been presented to solve the

geomechanical problems such as the simulation of shear band development [2, 12, 18, 28, 29]. Others were related to the theoretical investigation of the particle rolling on a flat surface [5] or the role of the rolling friction in granular packing [30]. The main objective of a large number of studies has been to reproduce a stable pile with a specific repose angle [9, 13, 20, 24, 27, 30]. Accordingly, it seems that the rolling resistance models are case specific. For example, the simulation results reported by the researchers have been shown that the group B models do not have the necessary efficiency to form a stable pile. In short, it could be stated that on account of complexity of the problem, there is no unique model for all applications (i.e. dynamic and pseudo-static regimes).

we believe that the best way to solve the problem of the ambiguity of the rolling friction model selection in the DEM relations is to evaluate the existing models and try to modify them regarding the objective of the research. In addition to the difficulty of selecting the optimal rolling friction model, the determination of the model parameters, such as rolling friction coefficient, and generally all the input simulation parameters (i.e., calibration) is a challenging step in DEM simulations [30-37].

1.2. Calibration of DEM simulations

Individual simple experiments such as the angle of repose (AoR) in various testing methods are commonly used as the reference for the calibration of cohesionless and free-flowing bulk materials [24, 27, 31, 32, 34, 36, 38, 39]. The common tests are lifting cylinder, shear box, hopper and draw down. Generally, the calibration is carried out by systematic variation of the parameters (i.e., trial-and-error) or using the optimization algorithms [40] until a suitable combination of input parameters is found. In other words, the key input parameters of DEM simulation (rolling and sliding friction coefficients) which mainly influence the macroscopic behavior of bulk materials are regularly changed until similar results to the laboratory tests are numerically replicated in DEM. Since the lifting cylinder, shear box and hopper tests describe only a pseudo-static regime, the draw down box focusing on both the dynamic and pseudo-static regimes is preferred by researchers [41].

A full access to an in-house developed DEM software (KMPC_{DEM}[©]) source codes enabled us to add or modify the algorithms and related

relationships. The objective of the present work was to assess the robustness of three models of rolling friction and calibration of input parameters by comparing the repose angle of iron ore pellets obtained through the draw down test in a laboratory setup. A well-accepted model of rolling friction was then modified and applied to DEM relations of $KMPC_{DEM}^{\circ}$. The simulation results showed that the modified model was able to produce high repose angles. Finally, a comparison of the calibrated DEM simulation and the laboratory results showed a good agreement.

2. Materials and methods

2.1. Experimental setup

The calibration experiments were conducted using the draw down test, representing the

discharge of a hopper. The dimensions of the experimental setup (including two boxes) are given in Figure 3-a. The depths were 100 mm and 160 mm for the upper and lower box, respectively. The outlet opening was set to a width of 110 mm. The overviews of the draw down test before and after opening the flap are shown in Figure 3-b. As a result, four experimental reference criteria (shown in Figure 4) in one test could be generated [41]. The criteria are the followings:

- AoR in the lower box (β_{DD})
- Mass flow rate (\dot{m}_{DD})
- Shear angle in the upper box (φ_{DD})
- Discharged mass in the lower box (m_{DD})

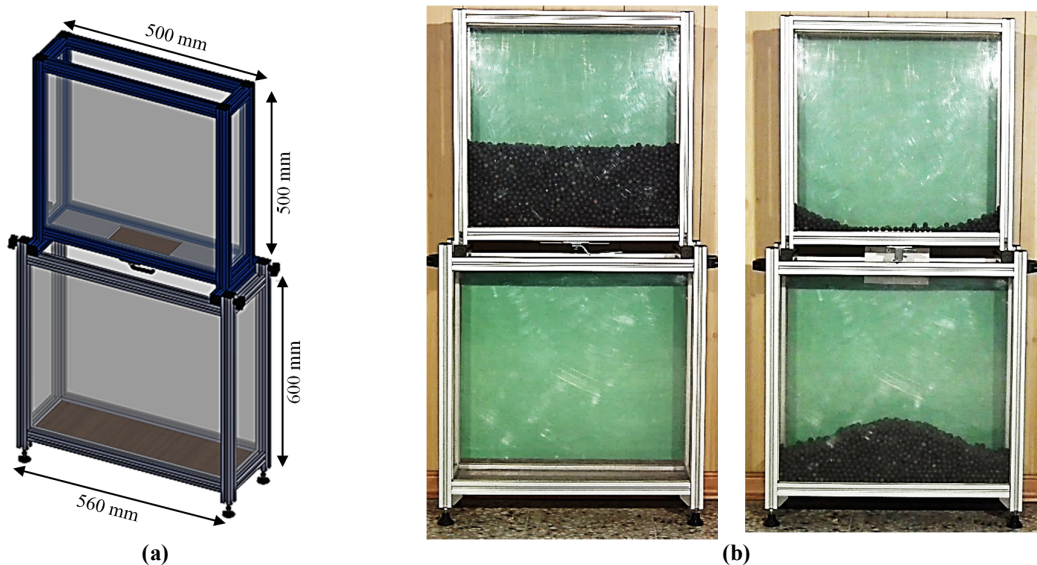


Figure 3. a) A 3D view of draw down test setup, b) An overview of the draw down test (for spherical plastic beads).

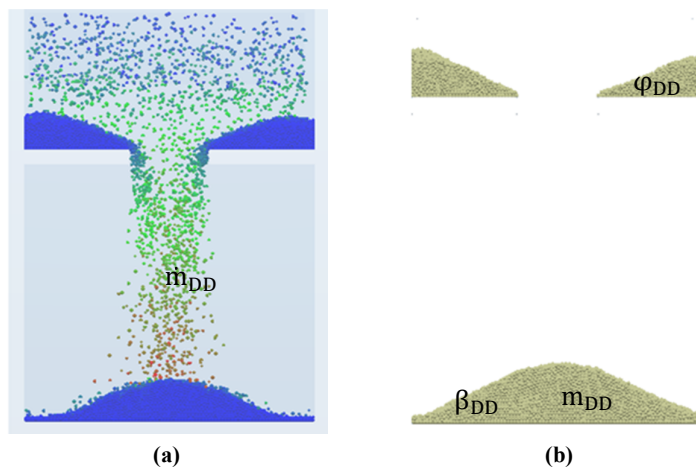


Figure 4. The schematic representation of the four criteria in the calibration process a) dynamic regime, b) static regime.

2.2. Experimental conditions and procedures

A sample of iron ore pellets classified as 17 mm (i.e., the top size) was used for the experimental investigations. The pellets generally have high porosity and a mechanical strength and low adhesion (Figure5). The material was easy to handle and represented a typical non-cohesive and free flowing material. Furthermore, this material is a common type that KMPC often deals with and it was required to characterize to find a DEM model for future works. The particle size distribution of the pellets is given in Table 1. The test was repeated three times to check the repeatability. The test procedure was filmed using a high-speed camera and, some photos were also taken.

Table 1. Particle size distribution of iron ore pellets.

Size (mm)	Fraction (%)
17	8
15	13
14	39
11	28
10	12

The repose and shear angles in photos were exactly measured in degrees by an electronic protractor goniometer (MB-Ruler version 5.0). The mass flow rate was estimated by image processing the films based on 2 seconds of entire falling time. In the conducted experiment, the discharged mass in the lower box was weighed.



Figure6. Sample of iron ore pellets.

2.3. Simulation conditions and procedures

For the numerical investigations, identical conditions (both setup and PSD) of the laboratory experiments were used for the simulations. Table 2 indicates the parameters used in the simulations. Considering the four criteria and based on trial-and-error procedure (at different coefficients of friction with 0.0001 intervals for rolling and 0.05 for sliding), the calibration was carried out. In this way, 35 simulations were required until a suitable combination of the rolling and sliding friction coefficients was found. After performing each simulation, three snapshots were taken and the repose and shear angles in the photos were measured. Knowing the position and velocity of all particles in DEM simulations, the mass flow rate was calculated for 2 s of simulation for the falling particles. The discharged mass in the lower box was calculated by means of the density and radius (i.e., volume) of the particles located in the lower box.

Table 2. DEM parameters used for the calibration simulations.

Parameter	Initial value	Calibrated value*	Unit
Number of particles		32370	
Density		7860	Kg/m ³
Elasticity modulus		0.24	MPa
Coefficient of rolling friction	0	0.0007	
Coefficient of sliding friction	0.5	0.75	
Coefficient of restitution		0.75	
Viscous rolling damping ratio		0.3	
J _n for calculation of rolling stiffness		0.4	
Cohesive force		0	N
Time step		1.7 × 10 ⁻⁴	s
Poisson's ratio		0.25	

*Explained in Section 3.2

3. Results and Discussion

3.1. Assessment of rolling friction models

The primary objective of the present work was to evaluate the performance of three more accepted models of rolling friction (i.e., models A, B, and

C). To this end, these models were investigated based on producing an AoR in the lower box for the static regime. Since we were interested in the overall understanding of the performance of models, we chose the scaled down setup (i.e., 1:10)

with low resolution to quickly perform the evaluation. In other words, three simulations (Figure 6) were conducted for 31886 mono-sized particles (i.e., 1.7 mm) and for a period of 20 s. The results obtained showed that for a given rolling friction coefficient (i.e., 0.1) these models could produce similar AoR in the lower box for the static regime, but only the type C model (elastic-plastic

spring dashpot model) provided a more stable shear angle in the upper box. It was in agreement with the researchers who had reported that the group C models could provide stable torques and appeared to work in various cases [12, 16, 41]. Accordingly, this well-accepted model was selected for more investigations in the dynamic regime.

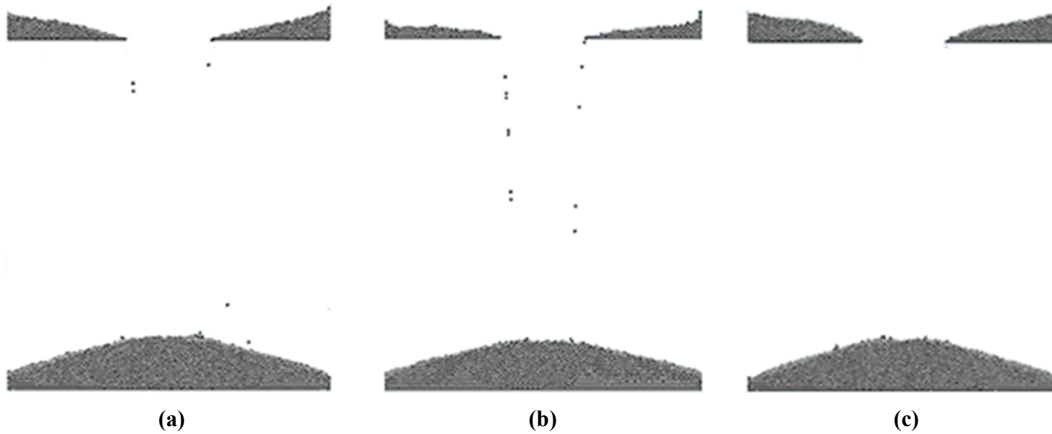


Figure 6. AoR tests - particle size: 1.7 mm - simulation time: 20 s - $\mu_r = 0.1$, a) type C model, b) type B model and c) type C model.

Figure 7 shows a comparison between AoR in the lower box for the dynamic regime at different rolling friction coefficients. Since this model could not produce relatively high repose angles (e.g., 29°

for the repose angle of iron ore pellets) even by using high values of rolling friction coefficient (e.g., 0.7), it was decided to modify the general form of the model.

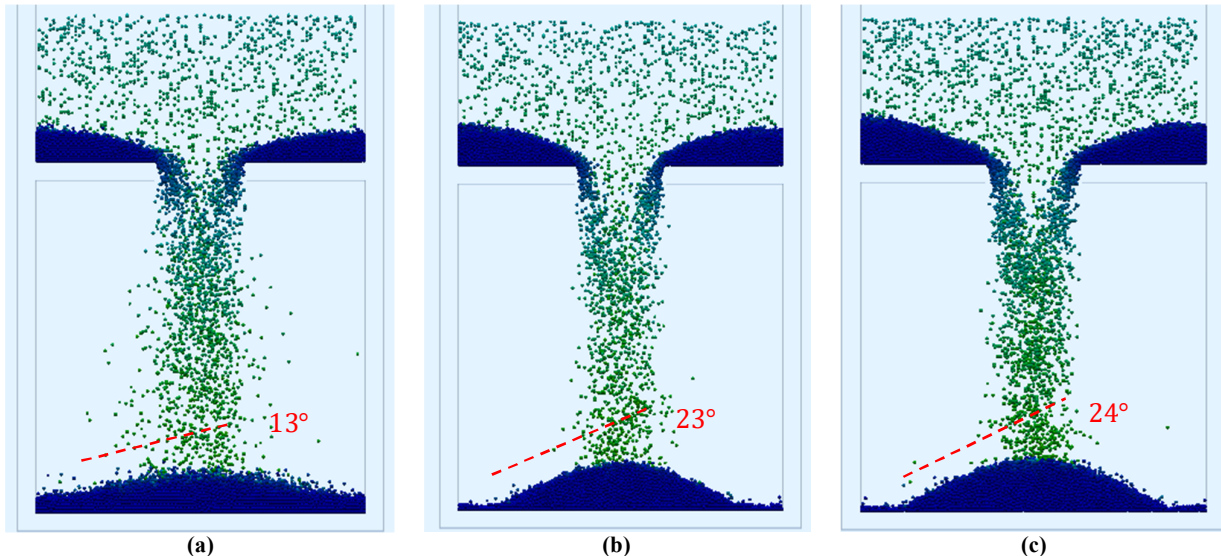


Figure 7. AoR tests - particle size: 1.7 mm - simulation time: 2 s - type C model, a) $\mu_r = 0$ (without applying the rolling friction model), b) $\mu_r = 0.1$ and c) $\mu_r = 0.7$.

Ai et al. [16] have claimed that the models in category D are not efficient since the contact pair torques are not at equilibrium. In all models, except for the group D models, the resistance torque is

applied as an equal to the particles forming the contact. In this manner, the variables (e.g., angular velocity, radius and moment of inertia) required to calculate the resistance torque are

considered as the relative quantities. It seems that referring to the Newton's third law the torque applies in this manner [17], while there is no rational reason to apply this law to moments like forces.

When the particle size distribution is narrow, the variables of particles such as linear and angular velocity during a simulation run are close to each other. Hence, using the relative parameters in resistance torques cannot create the sufficient friction in cases except facing collisions to stop the steady movement of particles by rolling. Accordingly, two different resistance torques must be applied to the particles forming the contact by considering the individual parameters instead of the relative values.

In spite of rejection of group D models by Ai *et al.* [16], the results of the present paper (Figure 8) showed that the modification of the group C models based on the concept of group D models could produce a higher AoR for a given rolling friction coefficient. By this approach, a fewer number of simulations is required to be performed in trial-and-error procedure (i.e., systematic variation of the parameters) for the calibration process because the desired similarity is faster observed. The general form of the modified model is similar to the group C models but the individual angular velocity, radius and moment of inertia of each of two contact entities are used instead of the relative angular velocity, effective radius and equivalent moment of inertia, respectively.

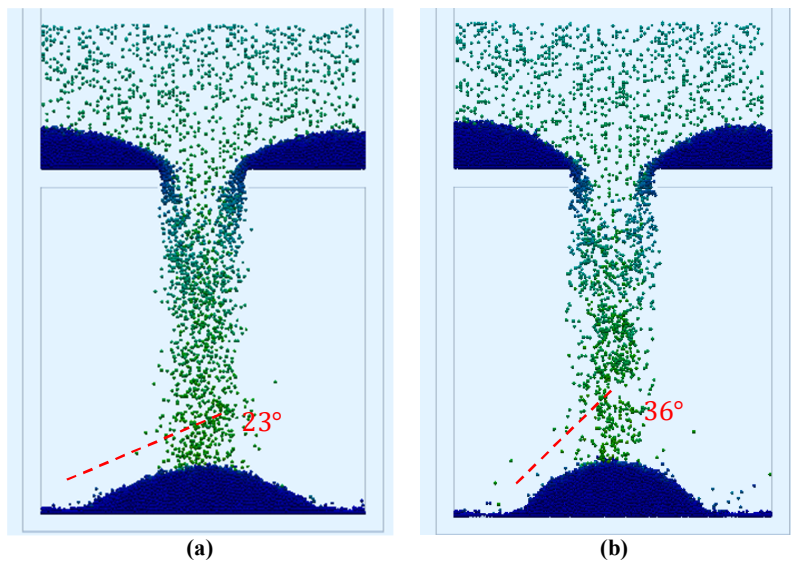


Figure 8. AoR tests - particle size: 1.7 mm - simulation time: 2 s - $\mu_r = 0.1$, a) type C model, b) modified type C model.

3.2. Calibration results

The modified model was exerted in the KMPC_{DEM} codes and then identical conditions (both setup and PSD) of the laboratory experiment were used for the calibration simulations. Table 3 provides a summary of four reference criteria measured in the laboratory setup and in simulations with only three combinations of rolling (μ_r) and sliding (μ_s) friction coefficients from 35 combinations. Each measurement was repeated three times (for both the left and right angles), and then the average and standard deviations (STD) were reported (Table 3).

The final results of the calibration for iron ore pellets using coefficient of sliding friction of 0.75

and coefficient of rolling friction of 0.0007 are shown in Figure 9. Comparison of the simulation and laboratory results showed a good agreement between the predicted and the measured angle of repose. The small differences seem to be originated from not considering the particle shape effects and assuming a spherical shape for particles. On the other hand, the shape can cause both rotation and resistance, whereas rolling friction always acts in the opposite direction of rolling motion. In this way, it is not unusual to observe somewhat higher angles in simulations in comparison to the real systems. The main outcome of this work could be stated as the accuracy of the simulation results considerably depending on the calibration process.

Table 3. Four reference criteria (simulation and experiment) at different combinations of rolling and sliding friction coefficients.

$\mu_r; \mu_s$		Simulation			Experiment
		0; 0.5	0.0003; 0.65	0.0007; 0.75	
β_{DD}	Average (deg.)	22.6	25.7	28.6	28.5
	STD (deg.)	0.4	0.9	0.8	1.0
φ_{DD}	Average (deg.)	16.6	20.4	36.8	35.5
	STD (deg.)	0.7	2.6	0.6	1.1
m_{DD}	Average (kg)	67.6	59.3	55.6	57.1
	STD (kg)	0.5	0.6	1.1	0.4
\dot{m}_{DD}	Average (kg/s)	4.5	4.0	3.1	3.5
	STD (kg/s)	0.8	0.8	1.0	0.5

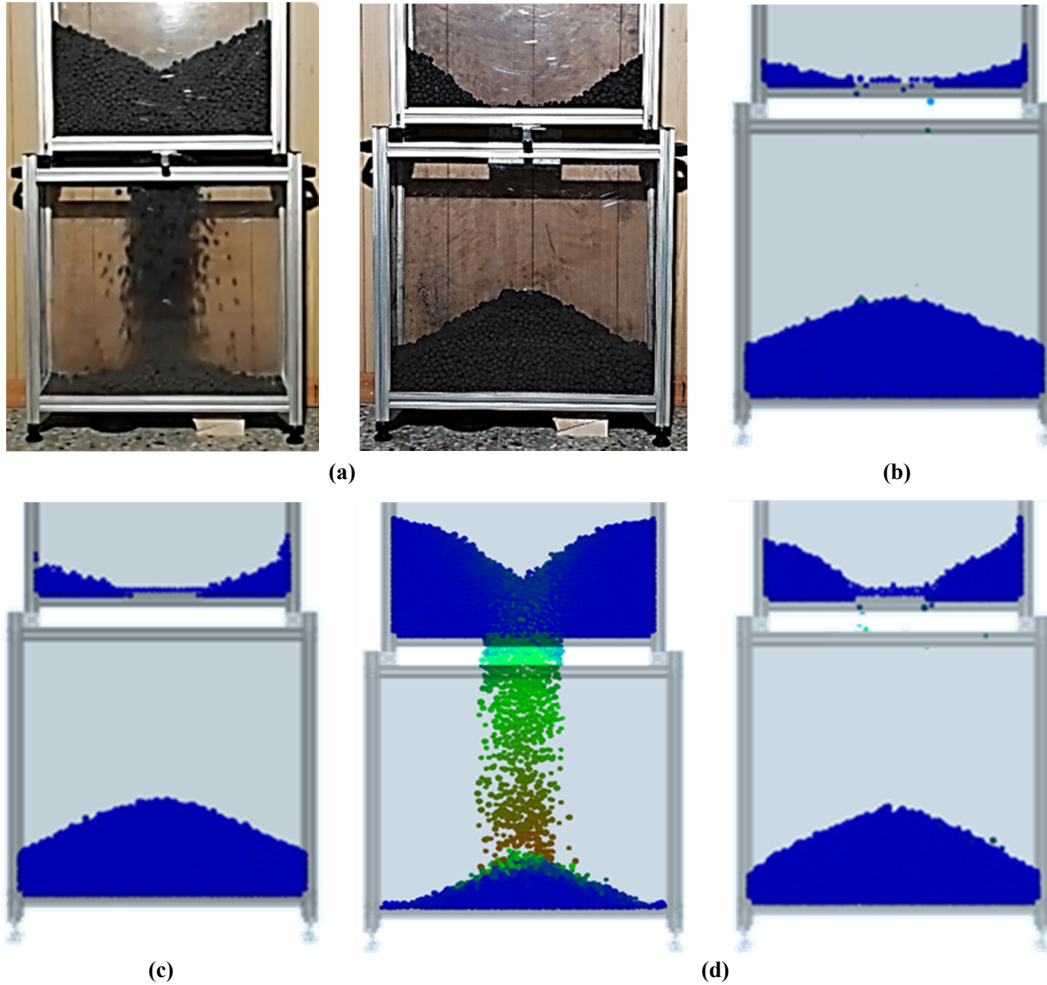


Figure 9. Results of the calibration: a) laboratory experiment, b) simulation using $\mu_r = 0$ and $\mu_s = 0.5$, c) simulation using $\mu_r = 0.0003$ and $\mu_s = 0.65$ and d) final simulation using $\mu_r = 0.0007$ and $\mu_s = 0.75$.

4. Conclusions

The in-house developed DEM software (KMPC_{DEM}[®]) was used to assess the robustness of three models of rolling friction. The results obtained showed that the modified elastic-plastic spring dashpot model could produce a more realistic angle of repose for iron ore pellets. By performing simulations, it was found that the coefficient of rolling and sliding frictions in the

case of pellets used in the work must be to 0.0007 and 0.75, respectively in order to make spherical particles to behave like a bulk material made up of real particles. Since the non-calibrated DEM simulations are prone to error, it is strongly recommended to use the laboratory experiments to characterize the materials before using the DEM simulation as a design tool in plants.

Acknowledgements

The authors would like to thank the Gol-E-Gohar mining and industrial company for supporting this research work. A special appreciation is also extended to Mr. Ansari as a member of the KMPC_{DEM} development group.

References

- [1]. Cundall, P.A. and Strack, D.L. (1979). A discrete numerical model for granular assemblies. *Geotechnique*. 29: 47-65.
- [2]. Iwashita, K. and Oda, M. (2000). Micro-deformation mechanism of shear banding process based on modified distinct element method. *Powder Technology*. 109: 192-205.
- [3]. Scharpf, D. (2008). DEM Applications: Simulation of Particulate Solids Handling and Processing Operations using the Discrete Element Method. *Vision of Engineering Analysis and Simulation: NAFEMS Company, Developer of EDEM Software*. 9-30.
- [4]. Coetzee, C.J. and Els, D.N.J. (2009). Calibration of discrete element parameters and the modelling of silo discharge and bucket filling. *Computers and Electronics in Agriculture*. 65: 198-212.
- [5]. Kondic, L. (1999). Dynamics of spherical particles on a surface: Collision-induced sliding and other effects. *Physical review E*. 60: 751-770.
- [6]. Grima, A., Hastiel, D., Curry, D., Wypych, P. and LaRoche, R. (2011). The beginning of a new era in design: Calibrated discrete element modelling. *Australian Bulk Handling Review*. 14-21.
- [7]. Hasankhoei, A.R., Maleki-Moghaddam, M., Haji-Zadeh, A., Barzgar, M.E. and Banisi, S. (2019). On dry SAG mills end liners: Physical modeling, DEM-based characterization and industrial outcomes of a new design. *Minerals Engineering*. 141: 105835.
- [8]. Ghasemi, A.R., Hasankhoei, A.R., Parsapour, Gh.A., Razi, E. and Banisi, S. (2020). A combined physical and DEM modelling approach to improve performance of rotary dryers by modifying flights design. *Drying Technology*. 1-18.
- [9]. Wensrich, C.M. and Katterfeld, A. (2012). Rolling friction as a technique for modelling particle shape in DEM. *Powder Technology*. 217: 409-417.
- [10]. Podlozhnyuk, A., Pirker, S. and Kloss, C. (2017). Efficient implementation of super quadric particles in Discrete Element Method within an open-source framework, *Computational Particle Mechanics*. 4: 101-118.
- [11]. Ghasemi, A.R., Razi, E. and Banisi, S. (2020). Determining a lower boundary of elasticity modulus used in the discrete element method (DEM) in simulation of tumbling mills. *Advanced Powder Technology*. 31: 1365-1371.
- [12]. Iwashita, K. and Oda, M. (1998). Rolling resistance at contacts in simulation of shear band development by DEM. *Journal of Engineering Mechanics*. 124 (3): 285-292.
- [13]. Zhou, Y.C., Wright, B.D., Yang, R.Y., Xu, B.H. and Yu, A.B. (1999). Rolling friction in the dynamic simulation of sandpile formation. *Physica A*. 269: 536-553.
- [14]. Bagi, K. and Kuhn, M.R. (2004). A definition of particle rolling in a granular assembly in terms of particle translations and rotations. *Journal of Applied Mechanics*. 71: 493-501.
- [15]. Sakaguchi, H., Ozaki, E. and Igarashi, T. (1993). Plugging of the flow of Granular materials during the discharge from a silo. *International Journal of Modern Physics B*. 7: 1949-1963.
- [16]. Ai, J., Chen, J-F., Rotter, J. M. and Ooi, J.Y. (2011). Assessment of rolling resistance models in discrete element simulations. *Powder Technology*. 206: 269-282.
- [17]. Wensrich, C.M., Katterfeld, A. and Sugo, D. (2014). Characterization of the effects of particle shape using a normalized contact eccentricity. *Granular Matter*. 16: 327-337.
- [18]. Zhao, C., Li, C. and Hu, L. (2018). Rolling and sliding between non-spherical particles. *Physica A*. 492: 181-191.
- [19]. Bardet, J.P. and Huang, Q. (1992), Numerical modeling of micropolar effects in idealized granular materials. *Mechanics of Granular Materials and Powder Systems*. 37: 85-92.
- [20]. Baxter, J., Tuzun, U., Burnell, J. and Heyes, D.M. (1997). Granular dynamics simulations of two-dimensional heap formation. *Physical review E*. 55: 3546-3554.
- [21]. Estrada, N., Azéma, E., Radjai, F. and Taboada, A. (2011). Identification of rolling resistance as a shape parameter in sheared granular media. *Physical Review E: Statistical, Nonlinear, and Soft Matter Physics*, American Physical Society. 84: 011306.
- [22]. Fukumoto, Y., Sakaguchi, H. and Murakami, A. (2013). The role of rolling friction in granular packing. *Granular Matter*. 15 (2): 175-182.
- [23]. Horabik, J., Parafiniuk, P. and Molenda M. (2017). Discrete element modelling study of force distribution in a 3D pile of spherical particles. *Powder Technology*. 312: 194-203.
- [24]. Zhou, C., Xu, B.H., ZOU, R.P., Yu, A.B. and Zulli, P. (2001). Stress distribution in a sandpile formed on a defected base. *Advanced Powder Technology*. 14: 401-410.

- [25]. Zhou, C., Xu, B.H., Yu, A.B. and Zulli, P. (2002). An experimental and numerical study of the angle of repose of coarse spheres. *Powder Technology*. 125: 45-54.
- [26]. Jiang, M.J., Yu, H.-S. and Harris, D. (2005). A novel discrete model for granular material incorporating rolling resistance. *Computers and Geotechnics*. 32: 340-357.
- [27]. Li, C., Honeyands, T., O'Dea, D. and Moreno-Atanasio, R. (2017). The angle of repose and size segregation of iron ore granules: DEM analysis and experimental investigation. *Powder Technology*. 320: 257-272.
- [28]. Oda, M., Konishi, J. and Nemat-nasser, S. (1982). Experimental micromechanical evaluation of strength of granular materials: Effects of particle rolling. *Mechanics of Materials*. 1: 269-283.
- [29]. Oda, M. and Kazama, H. (1998). Microstructure of shear bands and its relation to the mechanisms of dilatancy and failure of dense granular soils. *Geotechnique*. 48 (4): 465-481.
- [30]. Barrios, G.k.P., Carvalho, R.M., Kwade, A. and Tavares., L.M. (2013). Contact parameter estimation for DEM simulation of iron ore pellet handling. *Powder Technology*. 248: 84-93.
- [31]. Frankowski, P. and Morgeneyer, M. (2013). Calibration and validation of DEM rolling and sliding friction coefficients in angle of repose and shear measurements, Proc, 7th International Conference on Micromechanics of Granular Media (AIP 1542). pp. 851-854.
- [32]. Santos, K.G., Campos, A.V.P., Oliveira, O.S., Ferreira, L.V., Francisquetti, M. C. and Barrozo, M.A.S. (2014). DEM simulations of dynamic angle of repose of acerola residue: A parametric study using a response surface technique, Proc, XX Brazilian Congress of Chemical Engineering, Brazil.
- [33]. Boemer, D. and Ponthot, G.P. (2016). DEM modeling of ball mills with experimental validation: influence of contact parameters on charge motion and power draw. *Computational Particle Mechanics*. 4. <https://doi.org/10.1007/s40571-016-0125-4>.
- [34]. Cheng, N.S. and Zhao, K. (2016). Difference between static and dynamic angle of repose of uniform sediment grains. *International Journal of Sediment Research*. <https://doi.org/10.1016/j.ijsrc.2016.09.001>.
- [35]. Bablena, A. and Hungary, G. (2017). DEM Calibration: a complex optimization problem, International Conference on Control, Artificial Intelligence, Robotics & Optimization, Athens, Greece. pp. 198-201.
- [36]. Beakawi, H.M., Al-Hashemi, Baghabra, O.S. and Al-Amoudi, (2018). A review on the angle of repose of granular materials. *Powder Technology*. 330: 397-417.
- [37]. Alizadeh, M., Asachi, M., Ghadiri, M., Bayly, A. and Hassanpour, A. (2018). A methodology for calibration of DEM input parameters in simulation of segregation of powder mixtures, a special focus on adhesion. *Powder Technology*. 339: 789-800.
- [38]. Roessler, T. and Katterfeld, A. (2018). Scaling of the angle of repose test and its influence on the calibration of DEM parameters using upscaled particles. *Powder Technology*. 330: 58-66.
- [39]. Jin, F., Xin, H., Change, C. and Sun, Q. (2011). Probability-based contact algorithm for non-spherical particles in DEM. *Powder Technology*. 212: 134-144.
- [40]. Benvenuti, L., Kloss, C. and Pirker, S. (2016). Identification of DEM simulation parameters by Artificial Neural Networks and bulk experiments. *Powder Technology*. 291: 456-465.
- [41]. Roessler, T., Richter, C., Katterfeld, A. and Will, F. (2019). Development of a standard calibration procedure for the DEM parameters of cohesionless bulk materials – part I: Solving the problem of ambiguous parameter combinations. *Powder Technology*. 343: 803-812.

دقت شبیه‌سازی‌های روش اجزای گسسته: تأثیر اصطکاک‌های غلتشی و لغزشی مطالعه موردی: گندله‌های سنگ آهن

الهام نعمت‌الهی^۱، علیرضا قاسمی^۱، عرفان راضی^۲ و صمد بنیسی^{۳*}

۱- بخش مهندسی معدن، دانشگاه شهید باهنر کرمان، کرمان، ایران

۲- مرکز تحقیقات قرآوری مواد کاشی‌گر، کرمان، ایران

ارسال ۲۹/۱۰/۲۰۲۰، پذیرش ۲۲/۱۱/۲۰۲۰

* نویسنده مسئول مکاتبات: Banisi@uk.ac.ir

چکیده:

روش اجزای گسسته (راگ) به عنوان یک روش شبیه‌سازی رایج برای تأیید طراحی‌های صنعتی (از طریق ایجاد دید بصری از آنچه در تجهیزات رخ می‌دهد)، به طور گسترده مورد استفاده قرار می‌گیرد. اگرچه راگ یک ابزار قدرتمند برای طراحی است، اما به لحاظ محاسباتی یافتن مدلی که بتواند توصیف‌کننده تمام ویژگی‌های رفتاری ذرات واقعی باشد، دشوار و چالش‌برانگیز است. از این رو، محققین زیادی برای بدست آوردن نتایج نزدیک‌تر به واقعیت سعی کرده‌اند با ارائه مدل‌هایی برای یک گشتاور مخالف، با کاهش انرژی ذرات از غلتش آزادانه آن‌ها جلوگیری کنند. به دلیل پیچیدگی موضوع، تاکنون مدل منحصر بفردی که به خوبی هم شرایط پایدار و هم دینامیکی را پوشش دهد، ارائه نشده است. در این تحقیق، از یک نرم‌افزار بومی (KMPC^{DEM}) برای بررسی سه دسته مدل از طریق مقایسه زاویه قرار بدست آمده در آزمون جعبه تخلیه استفاده شد. مدل الاستیکی-پلاستیکی فنر و میراگر بر اساس در نظر گرفتن پارامترهای جزئی ذرات درگیر در برخورد به جای پارامترهای نسبی اصلاح شد. نتایج نشان داد که مدل اصلاح شده می‌تواند زوایای قرار بالاتری را بازتولید کند. این مدل در کالیبراسیون پارامترهای ورودی شبیه‌سازی زاویه قرار گندله‌های سنگ آهن در یک دستگاه آزمایشگاهی آزمون جعبه تخلیه استفاده شد. مقایسه نتایج آزمایشگاهی و شبیه‌سازی نشان داد که با استفاده از مقادیر ۰/۰۰۷ و ۰/۷۵، به ترتیب، برای ضرایب اصطکاک غلتشی و لغزشی می‌توان به تطابق خوبی دست پیدا کرد. چون نتایج شبیه‌سازی‌های بدون کالیبراسیون مستعد خطای بالایی هستند، توصیه اکید می‌شود که پیش از استفاده از نتایج شبیه‌سازی راگ برای طراحی‌های صنعتی، از آزمون‌های آزمایشگاهی برای خصوصیت‌سنجی ذرات مورد شبیه‌سازی استفاده شود.

کلمات کلیدی: روش اجزای گسسته (راگ)، پارامترهای برخورد، زاویه قرار، کالیبراسیون، گندله‌های سنگ آهن.